Synthesis and Characterization of Nanostructured $(Fe_{80}Ni_{20})_{1-x}Cr_x$ (x= 0, 4) Alloys Using Mechanical Alloying and Density Functional Theory

Seyed Farzad Dehghaniyan[1,*], Shahriar Sharafi[2]

* *farzaddehghaniyan@gmail.com*

[1] Department of Materials Science and Engineering, School of Engineering, Shiraz University, Shiraz, Iran

[2] Department of Material Science and Engineering, School of Engineering, Shahid Bahonar University of Kerman, Kerman, Iran

Abstract: Mechanical alloying was employed to synthesize a nanostructured alloy with the chemical formula of $(Fe_{80}Ni_{20})_{1-x}Cr_x$ (x= 0, 4). The microstructural and magnetic properties of the samples were investigated using scanning electron microscopy (SEM), X-ray diffraction (XRD), energy-dispersive X-ray spectroscopy (EDS), and a vibrating sample magnetometer (VSM). Additionally, theoretical calculations were performed using density functional theory (DFT) under the generalized gradient approximation (GGA). Simulations have demonstrated that an appropriate quantity of chromium (Cr) can dissolve within the BCC-Fe (Ni) structure, resulting in a favorable enhancement of the magnetic moment of the lattice. The XRD results indicated that after 96 hours of milling, Fe (Ni) and Fe (Ni, Cr) with a body-centered cubic (BCC) structure were formed. With increasing milling time, the grain size decreased while the microstrain increased. The saturation magnetization (Ms) of $Fe_{80}Ni_{20}$ composition increased up to 32 hours of milling, but further milling (up to 96 h) resulted in a decrease in the saturation magnetization However, for the $(Fe_{80}Ni_{20})_{96}Cr_4$ powders, milling up to 64 h caused a reduction in Ms. The coercivity (Hc) trend was different and increased with longer milling times (up to 96 h) for both compositions.

Keywords: Mechanical alloying, Saturation magnetization, Nanostructured alloy, Density functional theory.

1. INTRODUCTION

Mechanical alloying is an effective approach aimed at generating nanostructured solid-state alloys. This process uses a high-energy mill to repeatedly weld, fracture, and reweld powder particles [1, 2]. Mechanical alloying resulted in the development of nanostructured powders with unique structures and characteristics. This is the present state of nanotechnology, which has resulted in nanostructured materials such as Fe-Ni alloys [1-4].

Pure iron is an excellent ferromagnetic element with extremely low resistivity. Alloyed iron has better magnetic properties and lower losses than pure iron magnets, leading to devices with higher efficiency [5]. The presence of alloying elements helps to align the magnetic domains in the material, increasing its saturation magnetization. This allows the material to be magnetized more effectively, resulting in a stronger magnetic field. Additionally, these alloying elements can also improve the material's permeability, which measures its susceptibility to magnetization. A higher permeability means that the material can be magnetized more easily, ultimately improving its overall magnetic performance [6]. When multiple ferromagnetic components with known saturation magnetization values combine to form a solid solution, the magnetic characteristics of the alloy fluctuate linearly with the weight % added. Alloying Fe with Ni increases electrical resistivity and thereby minimizes hysteresis loss. Furthermore, the permeability and saturation magnetization rise when the Ni concentration in a solid solution increases [7, 8].

However, Cr with a BCC lattice structure is a weak antiferromagnetic at ambient temperature. The significant dissolution gap in the Fe-Cr phase diagram distinguishes it from other state systems, such as Fe-Ni, in which both are soluble at ambient temperature. On the other hand, the coexistence of distinct magnetic characteristics, Ferro and antiferromagnetic, resulted in the remarkable feature of magnetoresistance [9, 10]. According to the published study, mechanical alloying is preferable for stabilizing the BCC phase, while the fcc phase stabilization is substantially less visible, and the equilibrium solubility of Ni in alpha Fe-lattice is 10 and 20%, respectively [5]. H. Shokrollahi et al [11] demonstrated that incorporating Ni into Fe can promote magnetic permeability and saturation magnetization. Further research on Fe-Cr systems

1

reveals that the mechanical alloying approach is a suitable, simple, and effective way for synthesizing these alloys and introducing Cr into the Fe lattice, therefore lowering grain size [9]. Theoretical simulations of Luo's research on $Fe_{1.5}M_{0.5}CoSi$ (M= V, Cr, Mn, Fe) compositions demonstrated that doping of low valent elements resulted in changing band structures and improved spin polarization. However, the research on the magnetic properties of materials is complicated due to the influencing variables and the restricted research on the characteristics of these materials [12].

The magnetic property was estimated theoretically using first principles based on density functional theory (DFT), and the impacts of importing Cr to Fe (Ni) structure on saturation magnetization were studied.

The composition used for this investigation is $(Fe_{80}Ni_{20})_{96}Cr_4$, which is considerably different from all prior alloys in the Fe-Ni systems. The current study aims to determine the optimal ball milling conditions to prepare $Fe_{80}Ni_{20}$ and $(Fe_{80}Ni_{20})_{96}Cr_4$ powders and will explore the magnetic and structural behavior of $Fe_{80}Ni_{20}$ and $(Fe_{80}Ni_{20})_{96}Cr_4$ powders theoretically and experimentally.

2. EXPERIMENTAL PROCEDURES

A mixture of elemental powders from pure Fe (99.9% purity, particle size ≤100 μm), pure Ni (99.9% purity, particle size ≤10 μm), and pure Cr (99.6% purity, particle size ≤200 μm) were used to make $Fe_{80}Ni_{20}$ and $(Fe_{80}Ni_{20})_{96}Cr_4$ alloys with planetary ball mill. Under an argon atmosphere (99.9% purity), The powders were placed in a steel container containing steel balls, with a ball-to-powder weight ratio of 20:1. A planetary ball mill was used to grind the samples for 8, 16, 32, 64, and 96 hours at a rotating speed of 300 rpm. Milling was done in 1-hour milling and a 30-minute resting phase. Ethanol was used as a process control agent (PCA) up to 1 wt% of the powder combination was placed into the container.

The morphology of materials was studied using scanning electron microscopy (SEM) (Cam Scan mv2300). X-ray diffraction (XRD) tests were performed by Philips X'Pert High Score employing Cu K (= 0.1545 nm) radiation throughout a 15-110 2θ range to study the

structure and phase change of materials. At ambient temperature, magnetic characteristics were examined using a vibration sample magnetometer (VSM).

Bragg's law (nλ= 2d sinθ) was used to get the lattice parameter, and crystallite size and microstrains were calculated using the Williamson-Hall method [13].

The Quantum ESPRESSO (QE) software, which is based on the plain wave approach and the pseudopotential methodology was used to perform DFT calculations in this work [14-16]. The ultra-soft pseudopotentials (PBE approximation) were utilized, with a kinetic energy cutoff of 40 Ry for the electron wave function and 320 Ry for the electron charge density. In our simulations, we took collinear magnetism (Ferro and anti-Ferro structures) into consideration.

3. RESULTS AND DISCUSSION

3.1. Simulation Results

Before studying the magnetization of compositions with BCC structure, we first studied the binding energy per atom of structures [14]. The results for the binding energies per atom for the structures are defined as

$$E_b = \frac{E_{total} - [(n_A E_A) + (n_B E_B)]}{n_A + n_B}$$

Where:
- E_b is the binding energy
- E_{total} is the total energy of the system
- n_A and n_B are the number of atoms of elements A and B in the system, respectively
- E_A and E_B are the total energies of isolated atoms of elements A and B, respectively.

A system's binding energy per atom is a measure of its stability. A more stable system has a higher binding energy per atom Fig. 1 demonstrates binding energy per atom for compositions with different Cr additions. As shown in Fig. 1 The addition of Cr raises the composition's binding energy which is due to the low solubility of Cr in Fe lattice [9, 10].

To investigate Ms variations, models of $(Fe_{80}Ni_{20})_{1-x}Cr_x$ (x= 0, 4, 8, 10) are constructed, and the Bohr magneton is estimated using the density functional theory (DFT) of first principles. Fig. 2 depicts solid solution models with various compositions, representing the
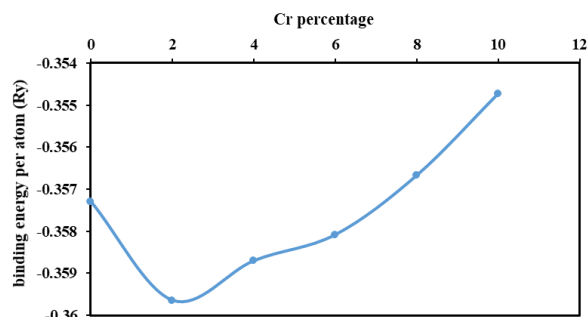
atomic ratio.

Fig. 1. Binding energy per atom versus different Cr addition percentage

The stability of the alloys was considered during the atom substitution procedure based on the binding energy. Fig. 3 depicts the fluctuation of the Bohr magneton of several solid solutions. It is clear that the proper amount of Cr solution in Fe (Ni) is beneficial for the increase of magnetic moment in Fe (Ni), but the excessive amount of Cr reduces magnetic. The reason for this is the electron distribution of Ni or Cr with Fe atoms, which causes the spin polarizability to grow and eventually affects the magnitude of the magnetic moment [17].

3.2. Microstructural Analysis

Mechanical alloying can significantly impact the shape and size of particles in SEM images, leading to a better understanding of the microstructural changes during the process. SEM images are used to observe the shape and size of powders; also, by using elemental maps, the purity and dispersal of elements are investigated. Fig. 4 shows the SEM images of $Fe_{80}Ni_{20}$ and $(Fe_{80}Ni_{20})_9Cr_4$ powders that were milled for 8, 16, 32, 64, and 96 h.

For both compositions, by milling up to 8 h, the ductile elements are flattened and constitute some big layered particles; also, a wide variety of particle sizes ranging from 10 to 50 μm can be observed [18]. During milling, particles get flattened, cold welding, fracturing, and rewelding continuously.

As shown in Fig. 4, after milling for up to 32 hours, the particles exhibit a broad range of sizes and a flak-like morphology, indicating that cold welding triumphs over fracture [19, 20]. The SEM images of $Fe_{80}Ni_{20}$ and $(Fe_{80}Ni_{20})_{96}Cr_4$ powders after 64 hours of milling demonstrate a more uniform distribution and smaller particle size compared to earlier milling durations.

This can be attributed to the prolonged milling process, which induces work hardening in the powders and enhances their resistance to deformation and fracture. Consequently, the primary mechanism during this stage is fracturing, leading to a reduction in particle size. For $(Fe_{80}Ni_{20})_{96}Cr_4$ milling up to 64 h leads to uniform distribution of powders due to work hardening as the dominance of fracturing over cold welding. Therefore, the size of particles is reduced, and the shape changes from flattened to round [19, 20]. Further milling up to 96 hours for both compositions results in reasonably homogenous particle size, which is explained by steady-state processing, welding, and fracture between work-hardened particles, while plastic deformation plays a minor role. [21].

Elemental maps were also used to investigate elemental distributions. After 64 hours of milling, all components of $Fe_{80}Ni_{20}$ and $(Fe_{80}Ni_{20})_{96}Cr_4$ alloys (Fig. 5 a and b) are uniformly dispersed, as shown in Fig. 5.
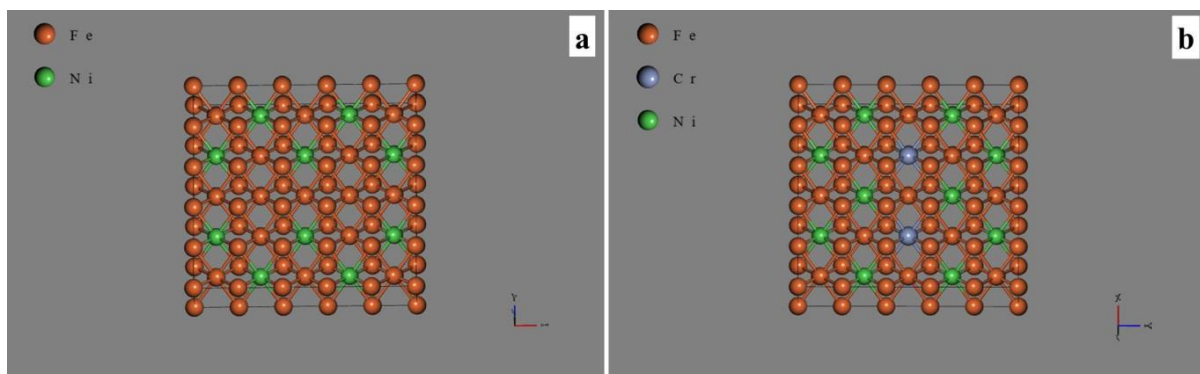

Fig. 2. Models of solid solutions with a) $Fe_{80}Ni_{20}$ and b) $(Fe_{80} Ni_{20})_{96}Cr_4$ compositions
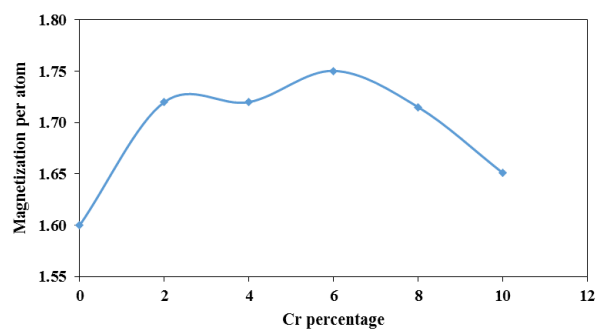
Fig. 3. Magnetization per atom versus different Cr addition percentage

Furthermore, the EDS elemental analysis for both compositions milled for 64 hours was done. The results are pretty close to the initial compositions. These analyses are 81.4 at. % Fe, 18.6 at. % Ni, for $Fe_{80}Ni_{20}$ composition and 78 at. % Fe, 17.5 at. % Ni and 4.5 at. % Cr, for $(Fe_{80}Ni_{20})_{96}Cr_4$ composition.

3.3. Phase Anaysis

Fig. 6 represents the X-ray diffraction patterns of $Fe_{80}Ni_{20}$ and $(Fe_{80}Ni_{20})_{96}$ Cr_4 milling for 0, 8, 16, 32, 64, and 96 h.

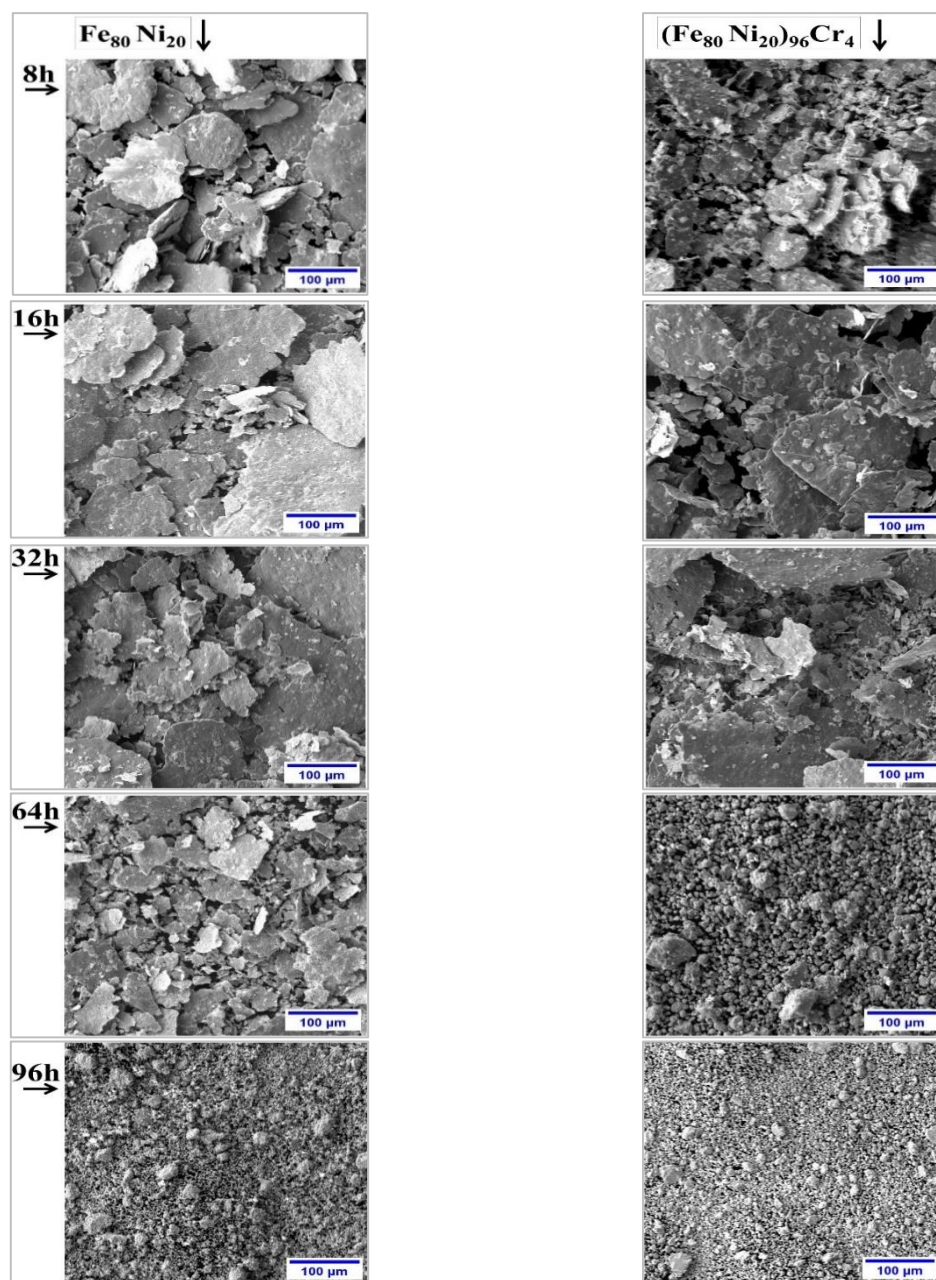**Fig. 4.** Sem images of $Fe_{80}Ni_{20}$ and $(Fe_{80}Ni_{20})_{96}Cr_4$ powders milled for different hours

4

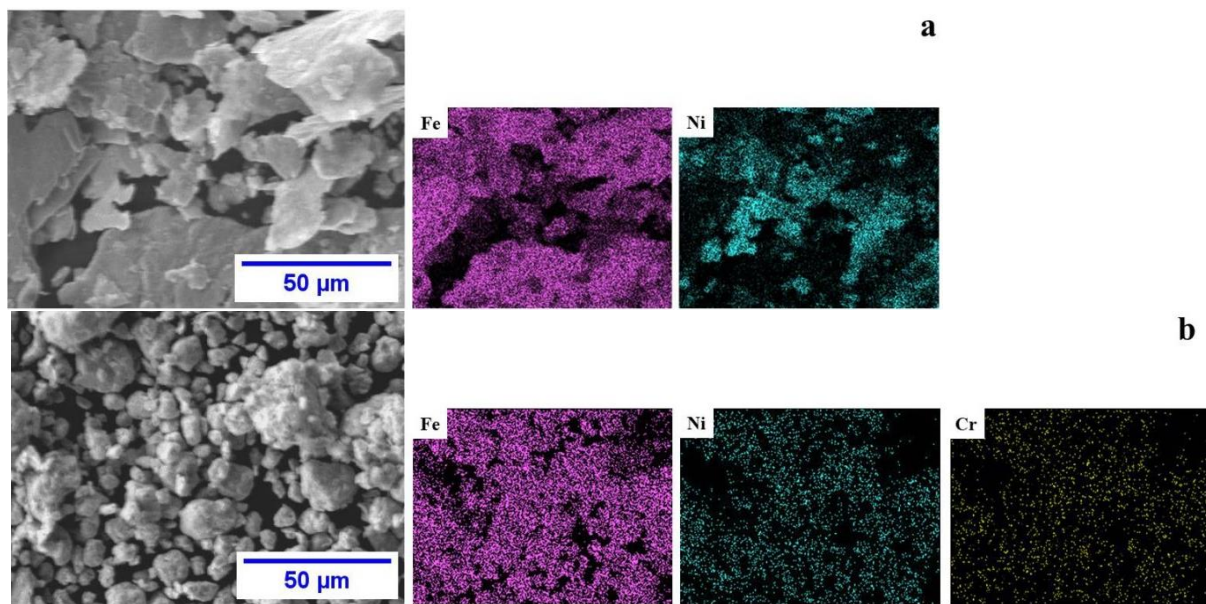**Fig. 5.** Distribution maps of Fe, Ni, and Cr in (a) $Fe_{80}Ni_{20}$ and (b) $(Fe_{80}Ni_{20})_{96}Cr_4$ milled for 64 hours

At the early milling stages, the XRD peaks indicate iron and chromium with BCC structures and nickel with fcc structures; furthermore, peaks of fcc-Ni diminish after 96 h milling for both compositions. For $Fe_{80}Ni_{20}$ (Fig. 6a), it is clear that Ni peaks decline gradually and vanish after 32 hours, a Fe (Ni) with a BCC structure appears, and Fe peak angles are low [1]. The XRD patterns of $(Fe_{80}Ni_{20})_{96}Cr_4$ milled for 8 and 64 h for 2 thetas between 63° and 67° are shown in Fig. 7. It is obvious that two peaks of Fe and Cr are visible after 8 hours, and the Cr peak declines after 64 h of milling, indicating that Cr atoms diffuse into the Fe (Ni) lattice. Thus, after 96 hours of milling, the BCC-Fe (Ni, Cr) solid solution formed. [22]. For both compositions, the peaks have narrowed with higher intensities due to temperature rises during milling from 8 to 16 h (Fig. 6). In general, the temperature of the powders during milling can rise for two reasons: a) it is due to the kinetic energy of the grinding process; and b) exothermic processes taking place during milling [1, 23].

The actual lattice parameter was the intercept of a graph drawn by the calculated lattice parameter (y-axis) versus the value of cos2h/sinh (x-axis) of each Braggs angle (high angles) [24]. The fluctuations in lattice parameter (a) with milling time (t) for $Fe_{80}Ni_{20}$ and $(Fe_{80}Ni_{20})_{96}Cr_4$ alloys are shown in Fig. 6. The lattice parameter for both compositions was reduced from 16 to 32 hours. This decline is ascribed to the diffusion of Ni atoms in substitution places of Fe lattice (since Ni's atomic radius is less than Fe's), as evidenced after 32 hours of milling when the Ni peaks are reduced, proving the lattice parameter results. [25, 26]. The lattice parameter increased from 32 to 96 hours of milling, caused by two reasons 1) diffusion of Ni atoms from alloy lattice to grain boundaries and 2) severe mechanical tension caused by the process. Because of the diffusion of Ni and/or Cr into the iron structure, the lattice parameter of $(Fe_{80}Ni_{20})_{96}Cr_4$ composition grows more than $Fe_{80}Ni_{20}$ in the final milling stages (32-96 h). Because Cr has a bigger atomic size than Ni, the $(Fe_{80}Ni_{20})_{96}Cr_4$ lattice parameter is higher than the $Fe_{80}Ni_{20}$. Table 1 shows the actual lattice parameter of compositions after 96 hours of milling contrary to simulation data of relaxed structures. As can be seen, experimental data have good agreement with computational data which indicates mechanical alloying process is completed after 96 hours of milling.

The Williamson-hall technique calculated crystallite size and lattice strain from XRD results [13]. Crystallite size fluctuates versus milling time in Fig 9. After 8 hours of milling, the crystallite size rapidly decreases for both compositions, caused by forming a solid solution. The crystallite size shows a steady fluctuation between 8 to 16 hours of milling due to the generation of defects such as dislocations [27].

The crystallite size reduces gradually as milling time increases, which the fetch process in three steps can describe. Firstly, deformation is focused

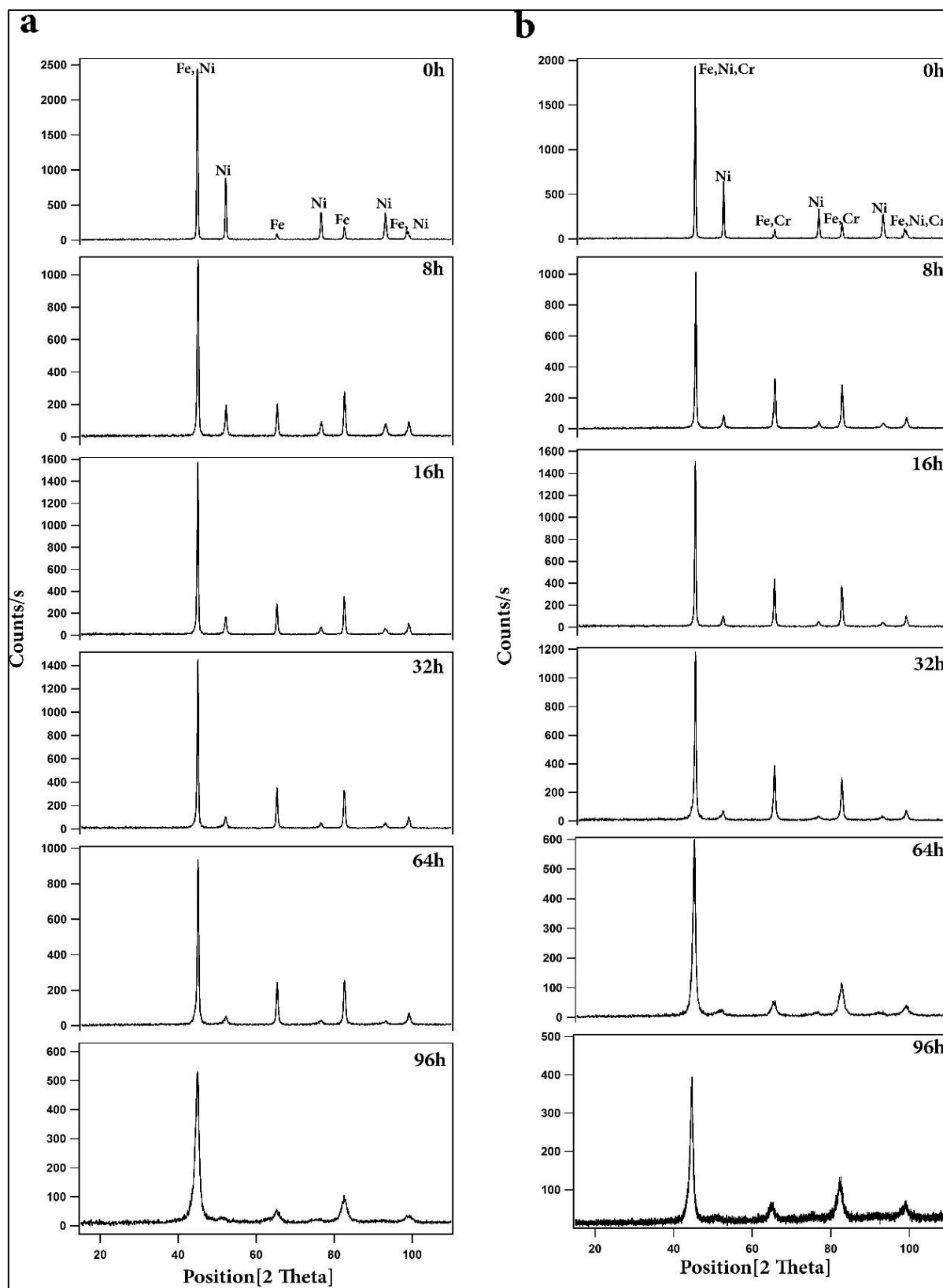on shear bands composed of a dense array of   dislocations.

Fig. 6. X-ray diffraction patterns of (a) $Fe_{80}Ni_{20}$ and (b) $(Fe_{80}Ni_{20})_{96}Cr_4$ powders milled for different hours
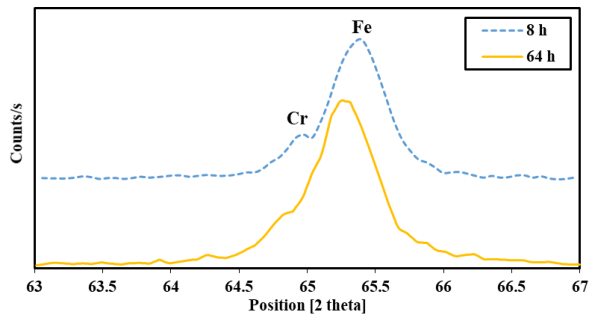
Fig. 7. X-ray diffraction patterns of $(Fe_{80}Ni_{20})_{96}Cr_4$ for 2 thetas between $63°$ and $67°$
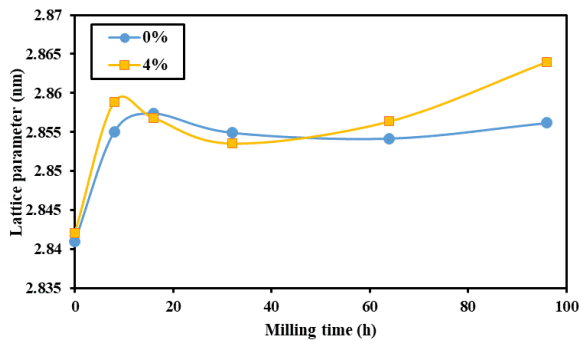

Fig. 8. Variations of lattice parameter versus different milling times for $Fe_{80}Ni_{20}$ and $(Fe_{80}Ni_{20})_{96}Cr_4$
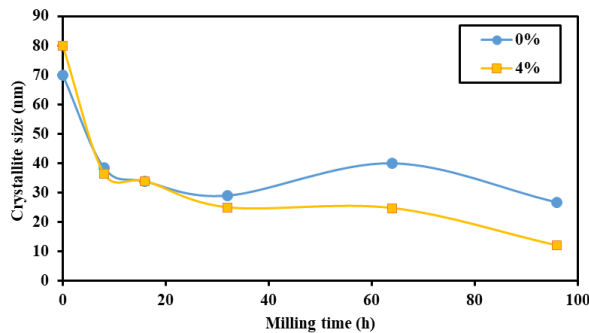

Fig. 9. Variations of crystallite size versus different milling times for $Fe_{80}Ni_{20}$ and $(Fe_{80}Ni_{20})_{96}Cr_4$

These dislocations then recombined to form low-angle grain boundaries that separated individual grains at a given strain level. Finally, the crystalline grains are randomly oriented with their neighbours [28]. The crystallite size rises between 32 to 64 hours due to recrystallization caused by the temperature increment of the system. Fig. 10 shows the micro-strain fluctuation over

different milling times. Mechanical alloying causes significant tension to be induced into the powders. As seen, crystal strain increased gradually over milling caused by mechanical alloying. Mechanical alloying generally provides considerable deformation through defects such as dislocations and stacking faults and a rise in the volume percentage of crystallite borders [1, 5].

Based on the coherent polycrystalline model, the volume fraction of the grain boundaries f_{gb} was approximated using the formula

$$f_{gb} = 1 - f_g$$

where f_g signifies the volume fraction of the grains provided by

$$f_g = \frac{(D - d)^3}{D^3}$$

And D is the size of the crystallite, and d is the effective grain-boundary thickness. The estimated thickness of the interfaces was generally found at 2-3 atomic layers in most of the nanostructured alloys, which is physically compatible with the thickness of the surface layer encountered in non-interacting nanoparticle systems [29, 30].
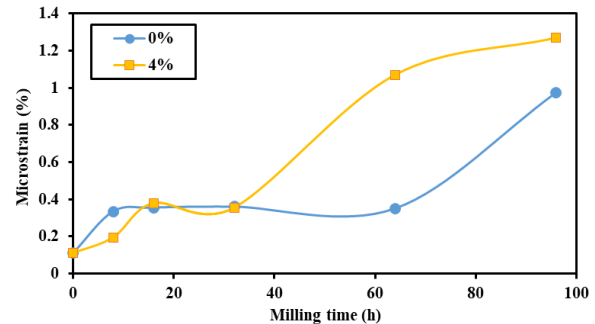

Fig. 10. Variations of internal micro-strain versus milling time for $Fe_{80}Ni_{20}$ and $(Fe_{80}Ni_{20})_{96}Cr_4$

The variation of the grain boundary fraction (f_{gb}) as a function of milling time is shown in Fig. 11. It has been demonstrated that when milling time increases, the fraction of grain boundaries increases and exceeds saturation in both compositions. Because of the potentially disordered structure of grain boundaries, increasing milling time will result in more defects being stored in grain boundaries [31].

Table 1. Actual lattice parameter of compositions after 96 hours of milling in contrary to simulation data of relaxed structures

composition	Lattice parameter (computation)	Lattice parameter (XRD results)	percentage error
0%	2.839	2.856	-0.56%
4%	2.939	2.864	2.55%
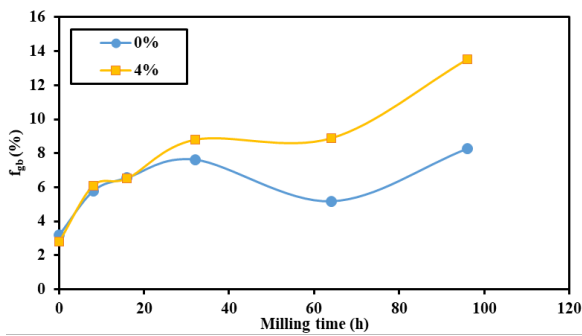
Fig. 11. Evolution of f_{gb} with milling time for $Fe_{80}Ni_{20}$ and $(Fe_{80}Ni_{20})_{96}Cr_4$

3.4. Magnetic Property Analysis

The saturation magnetization (Ms) graphing as milling time for both compositions in Fig. 12. The solid solution of BCC-Fe (Ni) and charge transfer between the ferromagnetic atoms can be attributed to the initial rise in Ms during 8 to 32 hours of milling in $Fe_{80}Ni_{20}$ composition. As demonstrated in Fig. 12, the saturation magnetization of $(Fe_{80}Ni_{20})_{96}Cr_4$ is lower than that of $Fe_{80}Ni_{20}$ during the early milling stages due to the chemical composition of the atom's surroundings. Cr is an antiferromagnetic element, as opposed to Fe and Ni, which are ferromagnetic. As a result, the Ms decrease is related to the presence of antiferromagnetic Cr atoms near Fe and Ni atoms and diminutions the magnetic moment of its neighbour atoms, reducing magnetization. Both compositions' saturation magnetization drops by further milling up to 96 h. The following factors might explain the drop in Ms: (a) a significant quantity of dissolved Ni and Cr in BCC-Fe. (b) magnetic atoms positioned in grain boundaries can reduce saturation magnetization. (c) Increasing the number of point defects, such as dislocations in the milling process, disrupts the domain walls' motion [32, 33].
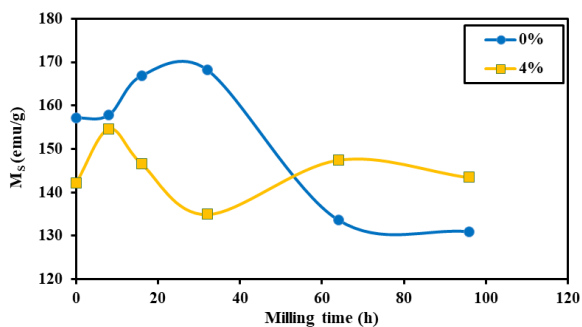

Fig. 12. Variations of saturation magnetization versus milling time for $Fe_{80}Ni_{20}$ and $(Fe_{80}Ni_{20})_{96}Cr_4$

Coercivity (Hc) is a critical parameter in soft magnetic materials. Defects such as grain boundaries, dislocations, and non-magnetic particles affect this magnetic property. Factors such as micro-strain, pores, and impurities introduced during mechanical alloying should be low to limit coercivity [11]. The coercivity varies with crystallite size (D) and Ms as follows:

$$H_c \approx 3\sqrt{\frac{KT_cK_1}{aM_s}}\frac{1}{D}$$

where D is the size of the crystallite, Ms is the saturation magnetization, K_1 is the magnetocrystalline anisotropy, Tc is the Curie temperature, K is the Boltzmann constant, and a is the lattice constant [34, 35].

In Fig 13, the coercivity fluctuates over milling time. As shown, the coercivity of the $Fe_{80}Ni_{20}$ composition remained constant for up to 64 hours of milling due to the equilibrium between defects generation and Ms increment. Fig 14 demonstrates the magnetic domains propagate over grains and grain boundaries. The coercivity of $(Fe_{80}Ni_{20})_{96}Cr_4$ rises to 32 hours of milling, as illustrated in Fig 14, for the following reasons. a) Cr atoms that are not dissolved in solid solution behave as inclusions, disrupting the mobility of domain walls [36] b) milling procedure increases microstrain and flaws [37].
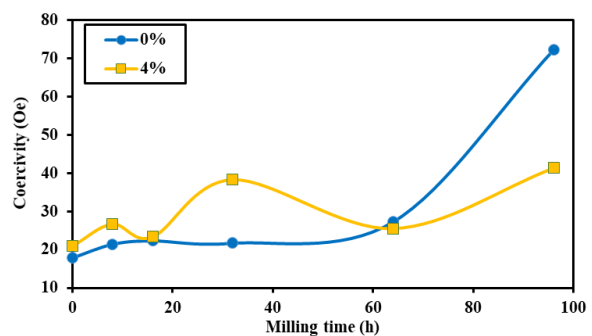

Fig. 13. Variations in coercivity versus milling time for $Fe_{80}Ni_{20}$ and $(Fe_{80}Ni_{20})_{96}Cr_4$

The coercivity of $(Fe_{80}Ni_{20})_{96}$ Cr_4 reduced from 32 to 64 hours of milling, which is thought to be attributable to a) during this time, the Cr and Ni atoms dissolve inside the solid solution and simplifying the domain walls motion, b) Also when the domain wall is larger than the grain size, Hc decreases significantly with decreasing grain size for nano-scale crystallite size [38]. After 96 hours of milling, for both compositions, the

coercivity rises due to the accumulation of lattice defects as a result of longer milling time.

The samples' hysteresis loops were measured and can be seen in Fig. 15. After 96 hours of milling, the saturation magnetization increased from 130 emu/g for the Fe (Ni) sample to 143 emu/g for the Fe (Ni, Cr) samples, and the coercivity reduced from 70 Oe to 40 Oe. The simultaneous increase in saturation magnetization and decrease in coercivity is attributed to an increase in both grain size reduction and Cr dissolution in the lattice.

4. CONCLUSIONS

Mechanical alloying with high-energy milling was used to obtain BCC $(Fe_{80}Ni_{20})_{1-x}Cr_x$ (x= 0, 4) solid solution powders. Powder shape distribution shifts from flattened to rounded form during mechanical alloying, and shape anisotropy reduces. The alloying of compositions with BCC structure was accomplished after 32 h and 64 h milling for $Fe_{80}Ni_{20}$ and $(Fe_{80}Ni_{20})_{96}Cr_4$, respectively, according to X-ray diffraction data. After 64 hours of milling, substantial changes in the lattice parameter of $(Fe_{80}Ni_{20})_{96}Cr_4$ were found, indicating that the Cr dissolved in the Fe-Ni lattice.
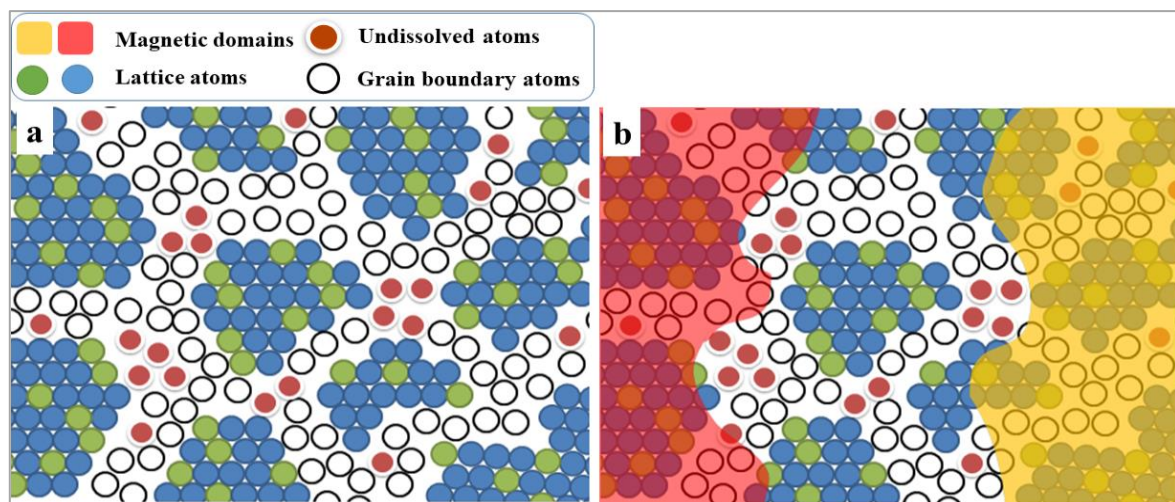

Fig. 14. Mechanism of magnetic domain propagation through grain boundaries a) before and b) after external field
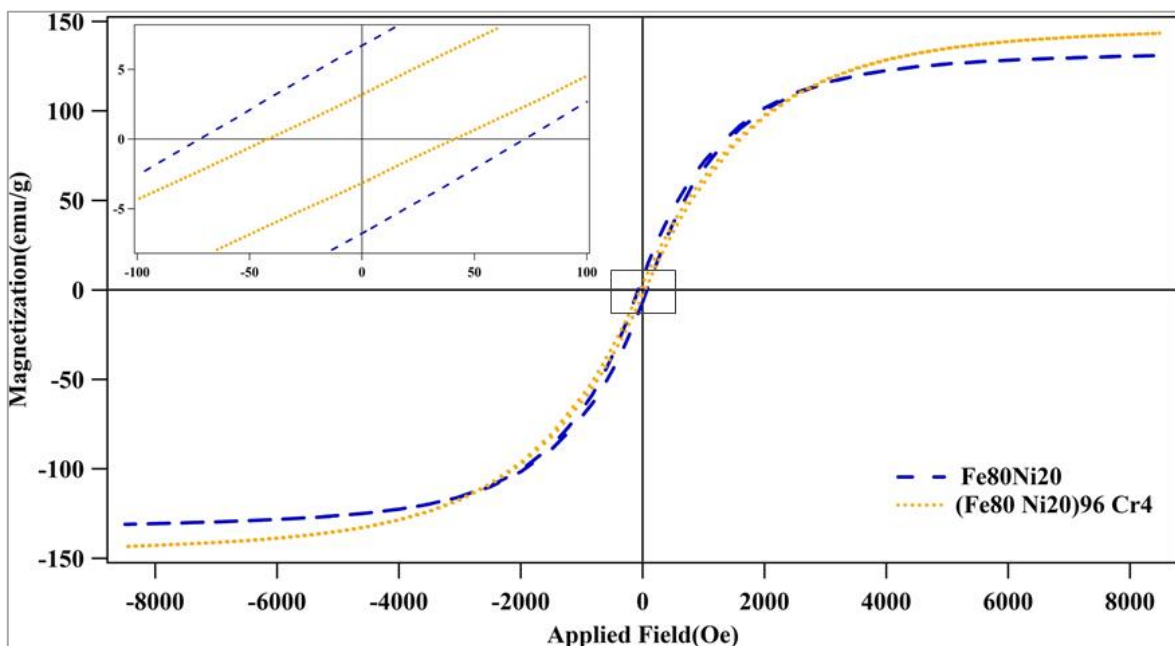

Fig. 15. Magnetization versus applied magnetic field for $Fe_{80}Ni_{20}$ and $(Fe_{80}Ni_{20})_{96}Cr_4$ milled for 96 hours

The results show that as milling time rose, crystallite size decreased continuously for both compositions and that adding 4% Cr enhanced crystallite size reduction rates. The density functional theory (DFT) demonstrated that a sufficient quantity of Cr solution in Fe-Ni is beneficial to improve magnetic in Fe (Ni), but an excessive amount of Cr lowers magnetic in Fe (Ni). Magnetic studies revealed that additional milling, up to 64 hours enhanced magnetization and coercivity of $(Fe_{80}Ni_{20})_{96}Cr_4$, while milling for further than 32 hours reduced the soft magnetic characteristics of $Fe_{80}Ni_{20}$. After 96 hours of milling, the saturation magnetization increases from 130 emu/g for the Fe (Ni) samples to 143 emu/g for the Fe (Ni, Cr) samples, and the coercivity reduces from 70 to 40. The simultaneous increase in saturation magnetization and decrease in coercivity is attributed to an increase in both grain size reduction and Cr dissolution in the lattice.

AUTHOR CONTRIBUTION

All authors contributed to the study's conception and design. Material preparation, data collection and analysis were performed by Seyed Farzad Dehghaniyan. The first draft of the manuscript was written by Seyed Farzad Dehghaniyan under the supervision of Shahriar Sharafi. All authors read and approved the final manuscript.

DATA AVAILABILITY

All data generated or analyzed during this study are included in this published article.

DECLARATIONS

The authors declare that they have no known competing financial interests or personal relationships that could have appeared to influence the work reported in this paper.

REFERENCES

[1]. Suryanarayana, C., Mechanical alloying and milling., Prog Mater Sci., 2001, 46, 1-184.

[2]. Hajalilou, A., Kianvash, A., Lavvafi, H., and Shameli, K. "Nanostructured soft magnetic materials synthesized via mechanical alloying: a review." J. Mater. Sci.: Mater. Electron., 2018, 29, 1690-1717.

[3]. Suryanarayana, C., Structure and properties of nanocrystalline materials., Bull. Mater. Sci., 1994, 17, 307-346.

[4]. Tcherdyntsev, V.V., Kaloshkin, S.D., Tomilin, I.A., Shelekhov, E.V., and Baldokhin, Y.V., "Formation of iron-nickel nanocrystalline alloy by mechanical alloying." Nanostructured Materials, 1999, 12, 139-142.

[5]. Koohkan, R., Sharafi, S., Shokrollahi, H., and Janghorban, K., "Preparation of nanocrystalline Fe–Ni powders by mechanical alloying used in soft magnetic composites.", J. Magn. Magn. Mater., 2008, 320, 1089-1094.

[6]. Pricop, V., Helerea, E., and Calin, M.D., "Influence of alloy elements on magnetic properties of electrical steels.", Int. Conf. Electr. Eng. Inform. Commun. Technol., Craiova, Romania, 2016, 1-6.

[7]. Jiles, D., Introduction to magnetism and magnetic materials. 1991, Chapman and Hall., Boca Raton, USA.

[8]. Jang, Y.I., Kim, J., and Hyuk Shin, D., "Microstructures and magnetic properties of amorphous Fe–Si–B–Ni alloy ribbons.", Mater. Sci. Eng. B, 2000, 78, 113-118.

[9]. Bentayeb, F.Z., Alleg, S., Bouzabata, B., and Grenèche, J.M., "Structural properties of Cr–Fe–Mn alloys prepared by mechanical alloying.", Physica B Condens. Matter, 2004, 351, 96-101.

[10]. Shen, G., Ma, X., and Shi, W., "Structural properties of Cr–Fe–Mn alloys prepared by mechanical alloying.", Physica B Condens. Matter, 2004, 351, 96-101.

[11]. Shokrollahi, H., "The magnetic and structural properties of the most important alloys of iron produced by mechanical alloying.", Mater. Des., 2009, 30, 3374-3387.

[12]. Yuping, D., Yahong, Z., Tongmin, W., Shuchao, G., Xin, L., and Xingjun, L., "Evolution study of microstructure and electromagnetic behaviors of Fe–Co–Ni alloy with mechanical alloying.", Mater. Sci. Eng. B, 2014, 185, 86-93.

[13]. Williamson, G.K., and Hall, W.H., "X-ray line broadening from filed aluminium and wolfram.", Acta Metall., 1953, 1, 22-31.

[14]. Giannozzi, P., Andreussi, O., Brumme, T., Bunau, O., Buongiorno Nardelli, M., Calandra, M., Car, R., Cavazzoni, C., Ceresoli, D., Cococcioni, M., Colonna, N., Carnimeo, I., Dal Corso, A., de Gironcoli, S., Delugas, P., DiStasio, R.A., Ferretti, A., Floris, A., Fratesi, G., Fugallo, G., Gebauer, R., Gerstmann, U., Giustino, F., Gorni, T., Jia, J., Kawamura, M., Ko, H.Y., Kokalj, A., Küçükbenli, E., Lazzeri, M., Marsili, M., Marzari, N., Mauri, F., Nguyen, N.L., Nguyen, H.V., Otero-de-la-Roza, A., Paulatto, L., Poncé, S., Rocca, D., Sabatini, R., Santra, B., Schlipf, M., Seitsonen, A.P., Smogunov, A., Timrov, I., Thonhauser, T., Umari, P., Vast, N., Wu, X., and Baroni, S., "Advanced capabilities for materials modelling with Quantum ESPRESSO.", J. Phys. Condens. Matter, 2017, 29, 465901.

[15]. Giannozzi, P., Baroni, S., Bonini, N., Calandra, M., Car, R., Cavazzoni, C., Ceresoli, D., Chiarotti, G.L., Cococcioni, M., and Dabo, I., "QUANTUM ESPRESSO: a modular and open-source software project for quantum simulations of materials.", J. Phys. Condens. Matter, 2009. 21, 395502.

[16]. Giannozzi, P., Baseggio, O., Bonfà, P., Brunato, D., Car, R., Carnimeo, I., Cavazzoni, C., De Gironcoli, S., Delugas, P., and Ferrari Ruffino, F., "Quantum ESPRESSO toward the exascale.", J. Chem. Phys., 2020, 152.

[17]. Wang, C.X., Lv, Z.Q., Fu, W.T., Li, Y., Sun, S.H., and Wang, B., "Electronic properties, magnetic properties and phase stability of alloyed cementite (Fe, M)3C (M= Co, Ni) from density-functional theory calculations.", Solid State Sci., 2011, 13, 1658-1663.

[18]. Suryanarayana, C., Mechanical Alloying and Milling., 2004, CRC Press.

[19]. Choo, K.S., Gheisari, K., Oh, J.T., and Javadpour, S., "Structure and magnetic properties of nanostructured $Ni_{0.77}Fe_{0.16}Cu_{0.05}Cr_{0.02}$ (Mumetal) powders prepared by mechanical alloying.", Mater. Sci. Eng. B, 2009, 157, 53-57.

[20]. Gheisari, K., Javadpour, S., Oh, J.T., and Ghaffari, M., "The effect of milling speed on the structural properties of mechanically alloyed Fe–45%Ni powders.", J. Alloys Compd., 2009, 472, 416-420.

[21]. Kim, S.-H., Lee, Y.J., Lee, B.-H., Lee, K.H., Narasimhan, K., and Kim, Y.D., "Characteristics of nanostructured Fe–33 at. % Si alloy powders produced by high-energy ball milling." J. Alloys Compd., 2006, 424, 204-208.

[22]. Louidi, S., Bentayeb, F.Z., Tebib, W., Suñol, J.J., Escoda, L., and Mercier, A.M., "Stacking faults and phase transformations study in ball milled $Co_{100-x}Cr_x$ (x= 0, 20, 50) alloys.", Mater. Chem. Phys., 2012, 132, 761-765.

[23]. Bahrami, A., Madaah Hosseini, H.R., Abachi, P., and Miraghaei, S., "Structural and soft magnetic properties of nanocrystalline $Fe_{85}Si_{10}Ni_5$ powders prepared by mechanical alloying.", Mater. Lett., 2006, 60, 1068-1070.

[24]. Khajepour, M., and Sharafi, S., "Structural and magnetic properties of nanostructured Fe 50(Co 50)–6.5 wt% Si powder prepared by high energy ball milling.", J. Alloys Compd., 2011, 509, 7729-7737.

[25]. Delshad Chermahini, M., Zandrahimi, M., Shokrollahi, H., and Sharafi, S., "The effect of milling time and composition on microstructural and magnetic properties of nanostructured Fe–Co alloys.", J. Alloys Compd., 2009, 477, 45-50.

[26]. Delshad Chermahini, M., Sharafi, S., Shokrollahi, H., Zandrahimi, M., and Shafyei, A., "The evolution of heating rate on the microstructural and magnetic properties of milled nanostructured $Fe_{1-x}Co_x$ (x= 0.2, 0.3, 0.4, 0.5 and 0.7) powders.", J. Alloys Compd., 2009, 484, 54-58.

[27]. Prasad, N.K., and Kumar, V., "Microstructure and magnetic properties of equiatomic FeNiCo alloy synthesized by mechanical alloying.", J. Mater. Sci.:

Mater. Electron., 2015, 26, 10109-10118.

[28]. Pan, H., He, Y., and Zhang, X., "Interactions between dislocations and boundaries during deformation.", Mater., 2021, 14, 1012.

[29]. Song, H., Guo, S., and Hu, Z., "A coherent polycrystal model for the inverse Hall-Petch relation in nanocrystalline materials.", Nanostructured Materials, 1999, 11, 203-210.

[30]. Pikula, T., Oleszak, D., Pękała, M., and Jartych, E., "Structure and some magnetic properties of mechanically synthesized and thermally treated Co–Fe–Ni alloys.", J. Magn. Magn. Mater., 2008, 320, 413-420.

[31]. Greneche, J.M., and Ślawska-Waniewska, A., "About the interfacial zone in nanocrystalline alloys.", J. Magn. Magn. Mater., 2000, 215, 264-267.

[32]. Hamzaoui, R., Elkedim, O., Fenineche, N., Gaffet, E., and Craven, J., "Structure and magnetic properties of nanocrystalline mechanically alloyed Fe–10% Ni and Fe–20% Ni.", Mater. Sci. Eng. A., 2003, 360, 299-305.

[33]. Hamzaoui, R., Elkedim, O., Gaffet, E., and Greneche, J.M., "Structure, magnetic and Mössbauer studies of mechanically alloyed Fe–20 wt.% Ni powders.", J. Alloys Compd., 2006, 417, 32-38.

[34]. Sourmail, T., "Near equiatomic FeCo alloys: Constitution, mechanical and magnetic properties.", Prog. Mater. Sci., 2005, 50, 816-880.

[35]. Prasad, N.K., and Kumar, V., "Structure–magnetic properties correlation in mechanically alloyed nanocrystalline Fe–Co–Ni–(Mg–Si)x alloy powders.", J. Mater. Sci.: Mater. Electron., 2016, 27, 10136-10146.

[36]. Farabi Khaneghahi, S., and Sharafi, S., "Magnetic and structural properties of nanostructured (Fe65Co35)100−xCrx (x= 0, 10) powders prepared by mechanical alloying process.", Adv. Powder Technol., 2014, 25, 211-218.

[37]. Chermahini, M.D., Sharafi, S., Shokrollahi, H., and Zandrahimi, M., "Microstructural and magnetic properties of nanostructured Fe and $Fe_{50}Co_{50}$ powders prepared by mechanical alloying.", J. Alloys Compd., 2009, 474, 18-22.

[38]. McHenry, M.E., Willard, M.A., and Laughlin, D.E., "Amorphous and nanocrystalline materials for applications as soft magnets.", Prog. Mater. Sci., 1999, 44, 291-433.